Applied Catalysis B: Environmental 154–155 (2014) 142–152

Contents lists available at ScienceDirect

Applied Catalysis B: Environmental

journal homepage: www.elsevier.com/locate/apcatb

ZnO-modified zirconia as gold catalyst support for the low-temperature methanol steam reforming reaction

Chongyang Wang, Matthew Boucher, Ming Yang, Howard Saltsburg, Maria Flytzani-Stephanopoulos*

Department of Chemical and Biological Engineering, Tufts University, 4 Colby Street, Medford, MA 02155, USA

ARTICLE INFO

Article history:
Received 7 November 2013
Received in revised form 28 January 2014
Accepted 4 February 2014
Available online 13 February 2014

Keywords:
Methanol steam reforming
Gold
Zirconia
Zinc oxide
Hydrogen

ABSTRACT

Nanoscale zirconia (ZrO_2) is widely investigated both as catalyst support and catalyst. Bare ZrO_2 binds gold weakly due to lack of surface defects. In this study, nanoscale ZrO_2 was modified with zinc oxide (ZnO) at different amounts, and examined as support of gold catalysts for the methanol steam reforming (SRM) reaction. ZrO_2 with high specific surface area serves as dispersant of ZnO to create highly dispersed ZnO clusters, which provide more anchoring sites for strong gold-metal oxide bonding. Addition of ZnO also passivates the surface acidity of ZrO_2, thus blocking the direct methanol decomposition to CO and H_2. To prepare the highly dispersed ZnO clusters on ZrO_2, a carbon hard-template method was used, followed by calcination at 550 °C to produce a highly porous mixed oxide solid. To investigate the modification of ZrO_2 by ZnO, the surface acidity was probed with isopropanol in temperature-programmed desorption (TPD) mode. Adsorption of the gold precursor on the ZnO-modified ZrO_2 was carried out by the anion adsorption method. Better dispersion, and better activity and stability of these gold catalysts were found than on either pure ZrO_2 or ZnO. Accordingly, the light-off temperature of SRM is lower and a wider temperature window for CO-free H_2 production up to moderately high temperatures (~375 °C) is found.

1. Introduction

As global energy demand continues to increase, development of alternative solutions for energy sustainability has attracted great attention. High on the list are fuel cells, the technology of which have made considerable advances in recent years [1]. Generation of high purity hydrogen [2] as feedstock is essential to the application of the proton exchange membrane fuel cells (PEMFCs). Because of current issues with the storage and transportation of gaseous hydrogen, however, methanol has been considered as a bridge-fuel for on-site reforming [3] to produce hydrogen. Methanol is attractive as a liquid fuel with relatively high energy density, high H/C ratio, and absence of C–C bonds, which enables its reforming at relatively low temperatures (200–300 °C) compared to ethanol (>400 °C) [2,4].

Hydrogen production from methanol can be carried out through methanol decomposition, steam reforming, partial oxidation, and autothermal reforming reactions [2]. Steam reforming of methanol (SRM) offers the highest H_2 yield among all the methanol conversion reactions [4]. The SRM reaction is endothermic [Eq. (1)]. SRM may also go through a first step of methanol decomposition reaction (DOM) [Eq. (2)] depending on the reaction conditions and different catalysts [4–6], which requires further conversion of the CO produced by the water gas shift reaction (WGS) [Eq. (3)]. Although the mechanism of the SRM reaction continues to be debated for certain catalysts, it is widely accepted that the conventional methanol synthesis catalysts, Cu/ZnO and $Cu/ZnO/Al_2O_3$, catalyze the SRM through coupling of the methoxy (CH_3O–) and formaldehyde (H_2CO–) intermediates without going through the DOM and WGS pathway [6–8]. Recent work from our group has focused on another Group I metal, gold, as a potential catalyst [9–11] for SRM to overcome the drawbacks of Cu catalysts; namely their pyrophoricity and deactivation at moderately high temperature. Importantly, Yi et al. [11] have shown gold to be equally selective to hydrogen as copper.

Studies of the partial oxidation of methanol by Friend and coworkers [12–14] have indicated the oxidative self-coupling mechanism of methanol on nanoscale gold catalysts, which is what was also found and reported the same year by Yi and co-workers for the SRM reaction on gold supported on ceria (CeO_2) [11,15]. A year later, Boucher and co-workers confirmed the same mechanism for gold supported on ZnO [9,10]. Availability of O-species on the support is critical to anchor and activate gold atoms for all

* Corresponding author. Tel.: +1 617 627 3048; fax: +1 617 627 3991.
E-mail address: maria.flytzani-stephanopoulos@tufts.edu
(M. Flytzani-Stephanopoulos).

http://dx.doi.org/10.1016/j.apcatb.2014.02.008
0926-3373/

methanol dehydrogenation reactions [9–11,15,16], as it is also for the water–gas shift reaction [9,17–19]. In the presence of methanol, however, the water–gas shift reaction pathway is shut-off at low temperatures (<250 °C) [11], hence the hydrogen selectivity of gold catalysts is as high as that of copper catalysts.

$$CH_3OH + H_2O \leftrightarrow CO_2 + 3H_2 \quad \Delta H_r = 49.7\,kJ\ mol^{-1} \tag{1}$$

$$CH_3OH \leftrightarrow CO + 2H_2 \quad \Delta H_r = 90.2\,kJ\ mol^{-1} \tag{2}$$

$$CO + H_2O \leftrightarrow CO_2 + H_2 \quad \Delta H_r = -41.2\,kJ\ mol^{-1} \tag{3}$$

In this work, nanoscale zirconia (ZrO_2) was investigated as a potential gold support for its good chemical and thermal stability [20]. ZrO_2 has been examined both as catalyst support and catalyst for various reactions. Bare ZrO_2 binds gold weakly and cannot stabilize it in atomically dispersed form under reaction conditions. Another issue with ZrO_2 is its strong Lewis acid sites, which favors the decomposition of methanol through η^2-adsorption [21] of the methoxy group, producing CO as an undesired intermediate. The Au/ZrO_2 system has been investigated for the CO oxidation [22,23] and the WGS reaction [24,25]. For the latter, Shen et al. [26] have proposed that the crystal phase of nanoscale ZrO_2 plays an important role in dispersing gold particles. Under-coordinated Zr(IV) in monoclinic ZrO_2 has a larger number of oxygen defects which can stabilize gold species better than tetragonal zirconia. In Boccuzzi and co-workers' research [24] on the WGS activity of Au/ZrO_2, it is argued that modification of the ZrO_2 surface with sulfate before addition of gold leads to a closer contact of gold with the support; i.e. better dispersion. One intriguing property of ZrO_2 is its amphotericity [27,28], which makes it a good candidate for bifunctional catalysis. Modulation of the surface acidity/basicity can benefit certain reactions by substantially improving the selectivity to the desired products. For instance, it was recently reported that suitably modified ZrO_2 with ZnO offers new possibilities for short-chain alcohol reforming reactions for the production of added-value chemicals, such as isobutylene [29]. It is thus interesting to us to use this approach in modulating the selectivity of the ZrO_2 surface to H_2 in the SRM reaction.

In this study, Au on bare ZrO_2 nanoparticles is observed to have unsatisfactory activity because of poor dispersion, and inferior selectivity to H_2 due to the strong surface acidity of ZrO_2 [30]. Modification of ZrO_2 with ZnO using a carbon hard-template method [29] was used to passivate the surface acidity of ZrO_2. The process was found to produce highly dispersed ZnO clusters in the ZrO_2 crystal domains. These ZnO clusters provide more oxygen defects for gold binding than unsupported bulk ZnO particles. Modified ZrO_2 with a suitable amount of ZnO thus has a much higher capacity to anchor and disperse gold atomically than either of the uncombined oxides. The resulting activity, selectivity, and catalyst stability are evaluated in this paper.

2. Experimental

2.1. Catalyst preparation

ZrO_2 and ZnO-modified ZrO_2 nanoparticles were prepared by adaptation of a carbon hard-template synthesis method [29]. ZnO nanoparticles were also prepared for comparison by the same method. The required amounts of zirconyl nitrate hydrate (Sigma-Aldrich, $ZrO(NO_3)_2 \bullet xH_2O$) and zinc nitrate hydrate (Sigma-Aldrich, $Zn(NO_3)_2 \bullet 6H_2O$) were dissolved in DI water to nominal Zn:Zr atomic ratios of 1:10 and 1:5. A solution of the precursor salts was then impregnated onto activated carbon (Sigma-Aldrich, Darco G-60) (Fe as impurity from the AC is under the detection limit of XPS and ICP) to incipient wetness endpoint. Two-step calcination was conducted at 400 °C for 4 h and 550 °C for 20 h in air. Gold was added on the supports by the anion-adsorption [31] method. Accordingly, 1 g of support powder was first suspended in 300 mL DI water at 80 °C. The gold precursor (Alfa-Aesar, $HAuCl_4 \bullet 3H_2O$) stock solution with concentration of 0.01 g/mL was added dropwise to the support suspension to reach 1 wt.% loading. The pH value of the suspension was monitored continuously, observing that pH of support suspensions were more than 2–3 units larger than the $HAuCl_4$ stock solution. $[AuCl_4]^-$ speciation ($[AuCl_4]^- + xOH^- \rightarrow [Au(OH)_xCl_{4-x}]^- + Cl_x^-$) took place at 80 °C under vigorous stirring for 4 h. The suspension was then filtered and washed with 1800 mL of DI water. The material was dried at room temperature under vacuum overnight, and calcined at 300 °C in 10% CO_2/He for 2 h.

2.2. Catalyst characterization

The BET surface area was measured by single-point N_2 physisorption cycles on a Micromeritics AutoChem II 2920. High-resolution transmission electron microscopy (HRTEM) was conducted on a JEOL 2010 electron microscope with 200 kV and 107 μA beam emission on as prepared gold-containing samples as prepared after calcination and used samples after SRM-TPSR to 400 °C. Aberration-corrected high-angle annular dark-field scanning transmission electron microscopy (ac-HAADF/STEM) images were obtained using a JEOL 2200FS STEM/TEM instrument equipped with a hexapole corrector (CEOS GmbH, Heidelberg, Germany) on the illuminating lenses. The corrector permits imaging at 200 kV in HAADF mode at a nominal resolution of 0.07 nm, with a collection semi-angle of 26.5 mr and a beam current of 23 pA. The gold loading capacity of each support was tested by inductively coupled plasma ion emission spectroscopy (ICP/IES) on a Leeman Labs PS1000 instrument. The collected filtrate after gold anion adsorption and washing was transferred into the argon plasma for the ICP measurement. Leachate of $Zn_1Zr_{10}O_x$ and Au-containing samples was also collected for ICP analysis. XRD analysis was performed on a Rigaku RU300 Cu-source powder diffractometer. Cu Kα radiation was used with a power setting of 50 kV and 250 mA. Scan rate of 2°/min with a 0.02° step size was used. X-ray photoelectron spectroscopy (XPS) was performed on a Thermo Scientific Al Kα-XPS. Surface titration tests with isopropanol were carried out in the temperature-programmed desorption (TPD) mode to probe the changes in the surface acidity/basicity of the ZnO-modified ZrO_2 samples. CO-temperature programmed reduction (CO-TPR) was conducted in 10% CO/He on all the gold-containing samples with ramping rate of 10 °C/min from 30 to 400 °C (holding at 400 °C for 30 min) to calculate the amount of active –OH groups. 3 cycles of CO-TPR were performed on each sample with room temperature rehydration and degassing in between cycles to study the regenerability of the –OH groups. Effluent gas was monitored online using a residual gas analyzer (SRS RGA 200).

2.3. Catalyst activity tests

The temperature-programmed and steady-state catalytic SRM reaction tests were carried out in a fixed-bed quartz microreactor (6 mm OD, 4 mm ID) at atmospheric pressure. Typically, 100 mg of catalysts in powder form were loaded in the quartz tube. The catalysts were diluted with 300 mg of quartz sand that was pretreated at 800 °C in air for 2 h. Catalysts were loaded to the reactor as calcined without any other heat treatment prior to reaction. For SRM-TPSR and SRM-steady state testing, a mixture of methanol and water was injected into a flow of pure He by a syringe pump and vaporized in the heated gas line before entering the reactor. The molar ratio of CH_3OH:H_2O:He was set to 2:2.6:95.4 and the total flow rate was set at 50 mL/min, corresponding to a gas hourly space velocity (GHSV) of 34,000/h (STP). The feed and the product gases were

Table 1
Physical and chemical properties of bare and ZnO-modified ZrO_2 nanoparticles.

Sample	ZnO	$Zn_1Zr_5O_x$	$Zn_1Zr_{10}O_x$	Leached-$Zn_1Zr_{10}O_x$	ZrO_2
Preparation procedure	AC-HT	AC-HT	AC-HT	AC-HT	AC-HT
Actual Zn:Zr by ICP	-	$Zn_1Zr_{3.7}$	$Zn_1Zr_{7.8}$	$Zn_1Zr_{13.3}$	-
Surface Zn:Zr atomic ratio by XPS	-	$Zn_1Zr_{2.5}$	$Zn_1Zr_{6.5}$	$Zn_1Zr_{35.4}$	-
S_{BET} ($m^2\ g_{cat}^{-1}$)	30	66	79	97	60
Point of zero charge	8.0–8.2	7.6–8.0	6.8–7.0	6.6–6.7	4.8–5.2
Crystal structure	h-ZnO	h-ZnO; t-ZrO_2	t-ZrO_2	t-ZrO_2	t-ZrO_2
Crystal size by XRD (nm)	35.1	7.8	5.6	7.1	8.1
Acetone selectivity (%)	83%	62%	60%	26%	14%
ZnO (%)	100%	20%	16%	0%	-
$ZnZrO_x$ mix (%)	-	80%	84%	100%	-
ZrO_2 (%)	-	0%	0%	0%	100%

[a] h-hexagonal, t-tetragonal, AC-HT: hard-template impregnation on activated carbon (Sigma-Aldrich, Darco G-60).

analyzed online by a residual gas analyzer (RGA, MKS model RS-1). The RGA was calibrated by monitoring a series of gases or vaporized liquid carried by ultra high purity He at different concentrations. The calibrated compounds for SRM include: CH_3OH (m/e = 31), H_2O (m/e = 18), CO (m/e = 28), CO_2 (m/e = 44), H_2 (m/e = 2), $HCOOCH_3$ (m/e = 60), CH_4 (m/e = 16). Compounds for isopropanol (IPA)-TPD include: acetone (m/e = 43), propylene (m/e = 41), isopropanol (m/e = 45), and isobutylene (m/e = 56). Several signals were corrected when cracking patterns of different compounds contributed to the same m/e value. The CO signal (28) was corrected for the contribution of methanol and CO_2 at m/e = 28. The propylene signal was corrected for the contribution of isobutylene and isopropanol at m/e = 41. Since acetone and isopropanol both contain m/e = 45 and 43 as cracking patterns, binary linear equations were solved to correlate the RGA signal intensity with compound concentration.

3. Results and discussion

3.1. Sample characterization

Physical and chemical properties of bare and ZnO-modified ZrO_2 are shown in Table 1. Actual Zn/Zr ratios of $ZnZrO_x$ composite oxides were measured by ICP and are listed in Table 1. Each sample was tested at least three times by ICP and the average value is listed in the table. ZrO_2 nanoparticles synthesized by the activated carbon hard-template method are highly crystallized in the tetragonal phase. Due to the similarity between the diffraction patterns of cubic and tetragonal phases of ZrO_2, the characteristic peaks of high index planes (400) at medium-angles (72–76°) were closely examined. As discussed by Srinivasan et al. [32], asymmetric doublets at ~74° indicate the tetragonal rather than the cubic phase of ZrO_2 (inset of Fig. 1). Moreover, synthesis of ZrO_2 from zirconyl precursors without structural stabilization by yttria or hafnia [33,34] typically produces the tetragonal phase of ZrO_2. $Zn_1Zr_5O_x$ and $Zn_1Zr_{10}O_x$ composite oxides synthesized by the activated carbon hard-template method demonstrate predominantly the tetragonal structure of ZrO_2, while ZnO hexagonal structure was also detected, see minor peaks in Fig. 1. Nanoscale ZnO polyhedra synthesized by the same method crystallize in the hexagonal system.

Addition of ZnO to ZrO_2 also modifies the surface chemistry of ZrO_2 by passivating the strong Lewis acid sites of ZrO_2 and simultaneously creating basic sites [29]. Significant increase (3–4 units) of point of zero charge (PZC) was observed by ZnO addition, which enables better speciation of $[AuCl_4]^-$ to $[Au(OH)_4]^-$ and facilitates the adsorption of the anionic gold precursor onto the positively charged metal oxide surface [35,36]. ICP analysis of the filtrate after 4 h of gold anion adsorption shows that the adsorption capacity for gold on $Zn_1Zr_{10}O_x$ was increased to 1.4 from 1 wt.% on bare ZrO_2. The designed amount of 1 wt.% gold loading was added to all the supports by the anion adsorption method. To study the effect of Zn addition on the performance of $ZnZrO_x$ as gold support, leaching of $Zn_1Zr_{10}O_x$ with 2 wt.% NaCN (~0.04 M) aqueous solution was carried out for 10 min to dissolve loosely bound ZnO particles. 42% of the original ZnO amount was leached off the $Zn_1Zr_{10}O_x$ sample, leaving the actual composition of the leached sample to be $Zn_1Zr_{13}O_x$. XPS analysis of all the supports was done to get the surface composition of Zn and Zr. The surfaces of $Zn_1Zr_5O_x$ and $Zn_1Zr_{10}O_x$ are slightly Zn-rich compared to the bulk Zn:Zr atomic

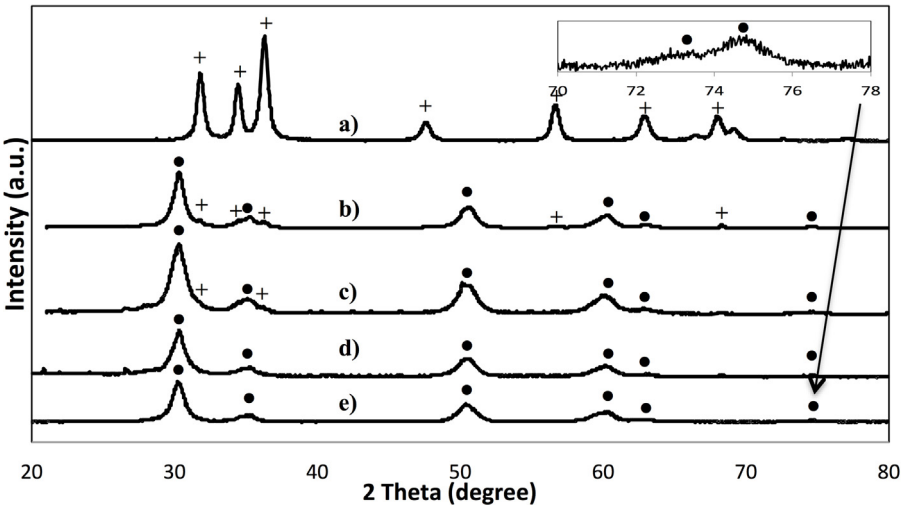

Fig. 1. XRD patterns of a) ZnO; b) $Zn_1Zr_5O_x$; c) $Zn_1Zr_{10}O_x$; d) Leached-$Zn_1Zr_{10}O_x$; e) ZrO_2.

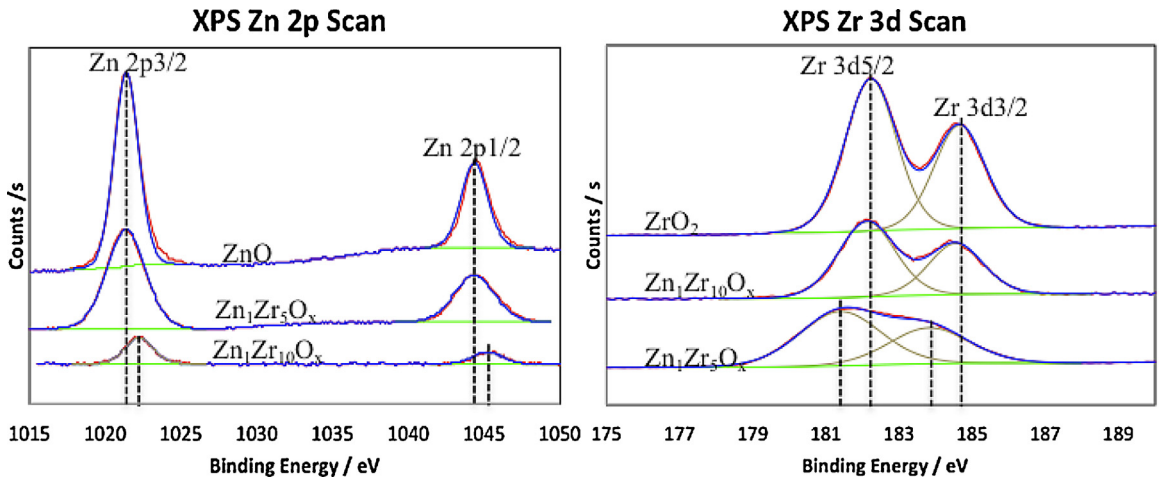

Fig. 2. XP spectra of ZnO, $Zn_1Zr_5O_x$, $Zn_1Zr_{10}O_x$, and ZrO_2 at Zn 2p binding energy range and Zr 3d range.

ratio (Table 1). XP spectra of Zn 2p show a binding energy shift on $Zn_1Zr_{10}O_x$ indicating the strong attachment between ZnO clusters and bulk ZrO_2. No shift was detected on the $Zn_1Zr_5O_x$ surface, which is consistent with masking effects by the high ZnO concentration in this and other such materials that we examined. However, here we can use the Zr 3d spectra to guide us. As shown in Fig. 2, there is a clear Zr 3d peak shift on $Zn_1Zr_5O_x$, where more (interfacial) ZrO_2 is in contact with ZnO (Fig. 2). Leaching of $Zn_1Zr_{10}O_x$ dissolved 42% of zinc in total, most of which from the surface, since the surface Zn:Zr atomic ratio of the leached $Zn_1Zr_{10}O_x$ significantly decreased from 1:13 (bulk) to 1:35. Interestingly, as will be discussed below, this small amount of ZnO associated with the ZrO_2 particles was enough to disperse the 1 wt.% gold atomically and create an active and stable SRM catalyst.

HR-TEM images of all the gold-containing samples, fresh and used (after SRM-TPSR to 400 °C), conducted on a JEOL 2100 microscope are shown in Fig. 3. No gold particles were visible in the fresh (calcined at 300 °C, in 10% CO_2/He, 2 h) samples of Au/ZrO_2, Au/leached-$Zn_1Zr_{10}O_x$, $Au/Zn_1Zr_{10}O_x$ and $Au/Zn_1Zr_5O_x$. However, gold particles can be clearly seen on the pure ZnO nanoparticles (~35 nm) even before reaction, due to the lack of adequate surface area (~30 m^2/g) to disperse all the gold added. Although no gold particles were imaged on the fresh Au/ZrO_2 sample, this could be partially due to the high electron density of ZrO_2 that might conceal the gold particles. Growth of gold into nanoparticles (>2.5 nm dia.) was detected on used Au/ZrO_2 and Au/ZnO samples. Milder agglomeration of Au into nanoclusters (1–2.5 nm dia.) was found on the modified supports, $Zn_1Zr_{10}O_x$ parent and its Zn-leached derivative, and $Zn_1Zr_5O_x$. Sintering of gold indicates destabilization under the reaction conditions. While the bulk ZnO nanoparticles were unable to keep most of the 1 wt.% Au in dispersed form, the $ZnZrO_x$ samples, where ZnO is highly dispersed itself as nanoclusters, allow the retention of gold in the active atomic state. To further investigate the dispersion of Au on ZrO_2 and Zn-modified supports, ac-HAADF/STEM was conducted on both the parent and leached Au/ZrO_2 and $Au/Zn_1Zr_{10}O_x$ as prepared samples at the Advanced Microscopy Laboratory in Oak Ridge National Laboratory, using a JEOL 2200FS STEM/TEM. Au particles on pure ZrO_2 are clearly seen along with gold atoms (Fig. 4a); while on $Zn_1Zr_{10}O_x$, only gold atoms were present (Fig. 4b). Leaching by 0.05% NaCN solution removed most of the gold particles from the Au/ZrO_2 sample (Fig. 4c), hence the image of the leached sample (Fig. 4c) shows only residual gold atoms. Leaching of $Au/Zn_1Zr_{10}O_x$ by NaCN aqueous solution also dissolved ~60% of Zn in the $Zn_1Zr_{10}O_x$ support (Table 2) along with the Au atoms attached to it. Atomically dispersed Au atoms species were still found to be the only form of Au on leached $Au/Zn_1Zr_{10}O_x$ (Fig. 4d).

3.2. Surface acidity/basicity titration by IPA-TPD

Isopropanol is a good probe molecule for surface acidity/basicity evaluation, since it dehydrates to propylene on strong Lewis acid sites [37], and dehydrogenates to acetone on weak Lewis acid sites and basic sites [38,39]. In our study, isopropanol-temperature programmed desorption (IPA-TPD) was performed on ZrO_2 nanoparticles containing different amounts of ZnO. 0.1 g of sample was loaded in a fixed bed quartz micro-reactor with 0.3 g of silica sand (pretreated at 800 °C in air for 2 h). Pure He gas carrying saturated isopropanol from a bubbler passed through the sample at a flow rate of 50 mL/min for 2 h, followed by He degassing overnight. A ramping rate of 2 °C/min starting from room temperature to 400 °C was used in the TPD experiments. The exit gas was continuously analyzed by the RGA. Considering acetone and propylene as the main products of isopropanol decomposition, and isobutylene as the secondary coupling product of acetone, He-carried vapor of isopropanol, acetone, propylene and isobutylene were calibrated in the same mass spectrometer to investigate the cracking patterns and sensitivity of the instrument to each product. To quantify the composition of different surface active sites based on the selectivity of IPA-TPD to different products within different temperature windows, experimental data of IPA-TPD were fitted, deconvoluted and integrated.

Acetone production on pure ZnO starts from 150 °C and peaks at 220 °C (Fig. 5-a), while on pure ZrO_2, it peaks at 320 °C (Fig. 3-b). Since both are amphoteric metal oxides, propylene was also produced, peaking at ~230 °C on ZnO and still at 320 °C on ZrO_2. IPA-TPD from $Zn_1Zr_{10}O_x$ (Fig. 5-d) shows two acetone peaks at 220 and 300 °C, respectively, and one propylene peak at 300 °C. The acetone and propylene peaks at 300 °C were not observed on either ZnO or ZrO_2, indicating the formation of a new type of active site on $Zn_1Zr_{10}O_x$. We propose that addition of ZnO at an atomic ratio of Zn:Zr = 1:10 will lead to two types of active sites on the surface: a small portion of ZnO particles that demonstrate the surface properties of pure ZnO; and a homogeneous composite of ZnO and ZrO_2 (denoted as $ZnZrO_x$) that exists in the form of highly dispersed ZnO clusters throughout the ZrO_2 phase. Isobutylene peaks (not shown in IPA-TPD/MS) observed at ~310 °C are likely due to the coupling of acetone produced at high temperature with water present on

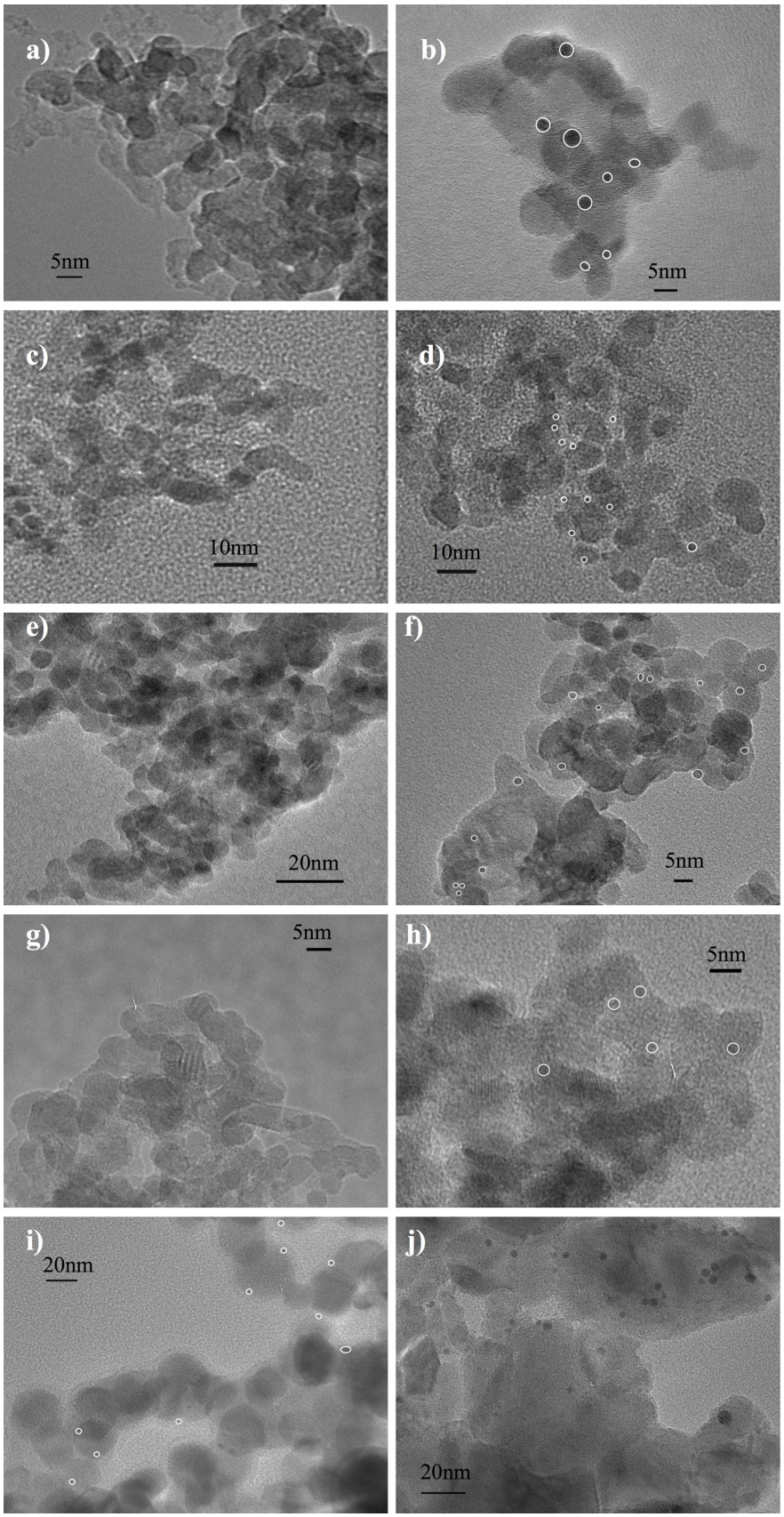

Fig. 3. HRTEM images of a-b) as prepared and used 1 wt.% Au/ZrO_2; c-d) as prepared and used 1 wt.% Au/leached-$Zn_1Zr_{10}O_x$; e-f) as prepared and used 1 wt.% $Au/Zn_1Zr_{10}O_x$; g-h) as prepared and used 1 wt.% $Au/Zn_1Zr_5O_x$; i-j) as prepared and used 1 wt.% Au/ZnO.

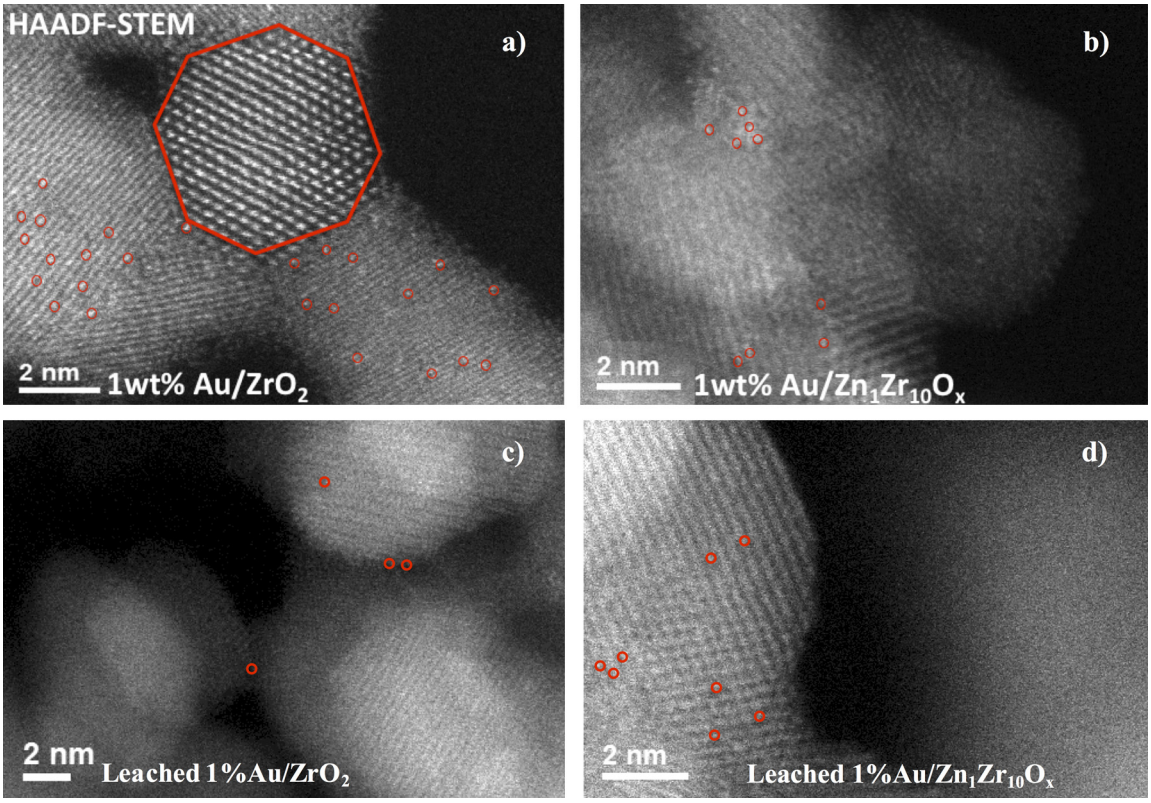

Fig. 4. ac-HAADF-STEM images of parent and leached Au/ZrO_2 (a, c); and parent and leached $Au/Zn_1Zr_{10}O_x$ (b, d). Circles are drawn around single gold atoms.

the surface [40]. A similar result was found on $Zn_1Zr_5O_x$ (Fig. 5-e). Acetone peak centered at 220 °C and propylene peak centered at 230 °C prove the existence of ZnO particles. With higher Zn concentration, t he amphotericity of ZnO is clearly demonstrated with both acetone and propylene peaks found at low temperature. High temperature peaks of acetone and propylene at ~300 °C indicate the formation of $ZnZrO_x$. Quantitation of each type of site is based on the integrated area of the product peaks..

It is interesting to find that the fraction of ZnO particles among the total active sites does not increase linearly with the ZnO amount in the bulk. To investigate the property of homogeneous composite of $ZnZrO_x$ in the ZnO-modified sample, sodium cyanide (NaCN) leaching was performed on $Zn_1Zr_{10}O_x$ to dissolve the ZnO particles that are not tightly bound with ZrO_2. 1 g of $Zn_1Zr_{10}O_x$ was suspended in 2 wt.% NaCN aqueous solution (pH ≥ 12) for 3 min, followed by filtering and washing with DI water until all Na was washed off from the sample. ICP test of the leachate reveals that 42% of Zn in $Zn_1Zr_{10}O_x$ was dissolved by the NaCN leaching. The leached-$Zn_1Zr_{10}O_x$ was tested by IPA-TPD/MS under the same condition, showing acetone and propylene peaks at ~300 °C only, hence containing the homogeneous $ZnZrO_x$ phase exclusively after leaching. The ZnO associated with this phase is not soluble in the highly alkaline solution.

3.3. Steady-state reaction tests

Methanol conversion over bare and ZnO-modified ZrO_2 and gold-containing samples was studied as a function of temperature. Temperature was ramped up at a linear rate of 5 °C/min, and held constant at each point shown for 2 h. Samples with same loading of gold on various supports with different Zn amounts were tested to investigate the effect of Zn content on the catalyst

Table 2
SRM reaction rates[e] on parent samples at 350 °C and rescaling of reaction rates based on the amount of Au atoms and active –OH groups[f].

Sample	1 wt.% Au/ZnO	1 wt.% Au/ZrO_2	1 wt.% $Au/Zn_1Zr_{10}O_x$	1 wt.% Au/leached $Zn_1Zr_{10}O_x$
Au in 1800 ml AA filtrate (ppm)	0	0	0	0
Au in 600 ml leachate (ppm)	3.68 ± 0.01	2.75 ± 0.02	2.52 ± 0.02	1.96 ± 0.01
Zn in 600 ml leachate (ppm)	6.92 ± 0.02	0	7.44 ± 0.06	0.73 ± 0.01
Percentage of Au retained	11.7%	33.0%	48.1%	53.2%
CO_2 production rate[a] at 350 °C (μmol/s/g_{cat})	1.76	3.09	7.44	6.23
CO:CO_2 selectivity at 350 °C	28:72	7:93	0:100	12:88
TOF(Au)[b] at 350 °C (s^{-1})	0.30 ± 0.03	0.18 ± 0.04	0.23 ± 0.07	0.30 ± 0.03
–OH group (μmol/g)[c] - parent	199	395	684	739
–OH group (μmol/g)[c] - leached	161	297	333	635
TOF(–OH)[d] at 350 °C (s^{-1})	0.009	0.008	0.011	0.008

[a] μmol of CO_2 produced per gram of catalyst per second.
[b] CO_2 molecules produced per gold atom per second.
[c] μmol of –OH groups per gram of catalyst up to 400 °C, Fig. 8.
[d] CO_2 molecules produced per active –OH group per second.
[e] SRM reaction rate was measured for $MeOH/H_2O$/He gas mixtures of molar ratio of 2/2.6/95.4.
[f] Amount of –OH groups is integrated of CO-TPR profiles from 30 up to 400 °C as shown in Fig. 8.

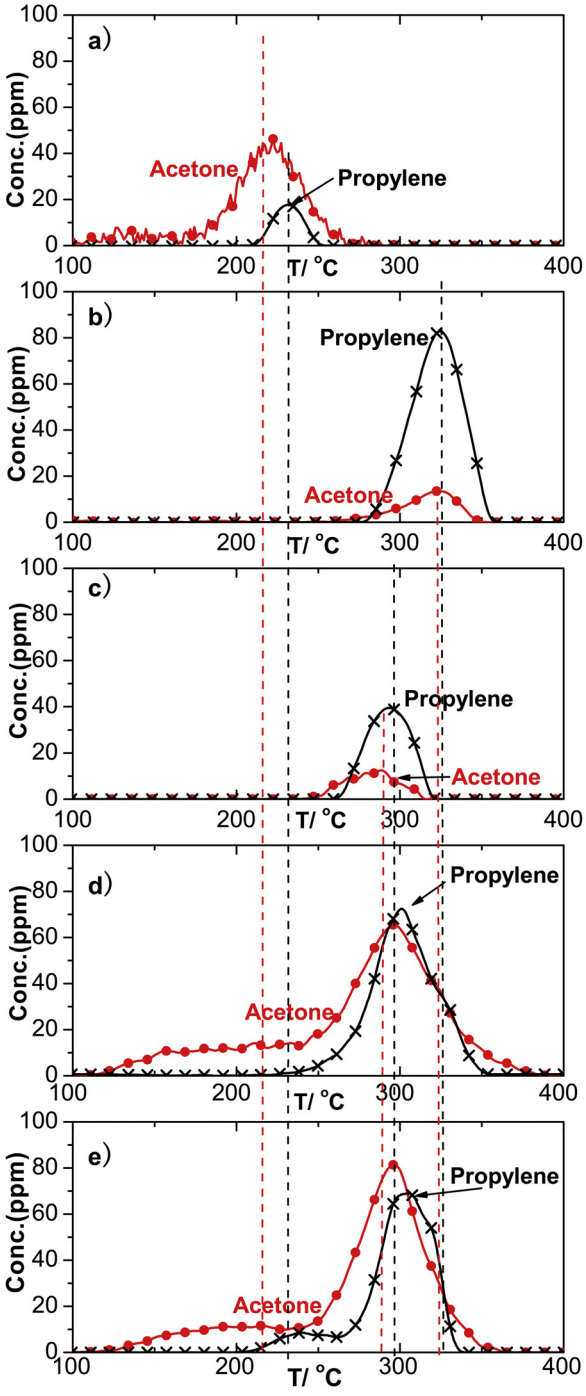

Fig. 5. Mass spectra from IPA-TPD on: a) ZnO (polyhedra); b) ZrO_2 (tetragonal); c) Leached-$Zn_1Zr_{10}O_x$; d) $Zn_1Zr_{10}O_x$; e) $Zn_1Zr_5O_x$.

activity (Fig. 6). Addition of gold lowered the light-off temperature of methanol conversion to as low as 200 °C on the leached $Zn_1Zr_{10}O_x$, the most significant effect shown among all gold-containing samples. Full conversion of methanol was reached at 400 °C on 1 wt.% Au/$Zn_1Zr_{10}O_x$, 1 wt.% Au/leached-$Zn_1Zr_{10}O_x$ and 1 wt.% Au/$Zn_1Zr_5O_x$, while 92% conversion of methanol was measured on 1 wt.% Au/ZrO_2 and 89% conversion on 1 wt.% Au/ZnO at 400 °C (Fig. 6). Superior activity was observed on gold catalysts supported on ZnO-modified ZrO_2. As mentioned above, $ZnZrO_x$ composite oxides with highly dispersed ZnO clusters create more active sites for SRM by better anchoring gold and keeping it atomically dispersed. This is consistent with the fact that no severe agglomeration of gold into particles was detected on the used samples supported by $Zn_1Zr_{10}O_x$, leached-$Zn_1Zr_{10}O_x$ or $Zn_1Zr_5O_x$ by HRTEM (Fig. 3-d, f, h).

To test the stability of the samples under reaction conditions, the samples were cooled down to 350 °C and held there for 2 h after reaching the highest temperature of 400 °C. These are shown by the filled symbols in Fig. 6. The conversions of methanol were in close agreement on Au catalysts supported by $Zn_1Zr_{10}O_x$, leached-$Zn_1Zr_{10}O_x$ and $Zn_1Zr_5O_x$; a considerable deactivation occurs on the Au/ZrO_2 sample after reaching the highest temperature of 400 °C. This is attributed to the loss of atomically dispersed gold from this sample after use at 400 °C (Fig. 3a-b). Au/ZnO on the other hand shows a slight increase of methanol conversion for the second run, which might due to the promotion effected by the production of H_2 at high temperature (400 °C) for the Au/ZnO system as reported by Boucher and co-workers [10].

Steady-state SRM reaction rate data were collected to calculate the activation energy of the reaction on the bare supports and the gold-containing samples. Conversions were kept low (<20%) to approach differential reactor conditions. Yi et al. first reported the apparent activation energy of SRM on highly dispersed gold on ceria (CeO_2) to be 110 ± 1.2 kJ/mol [11,15]. Boucher et al. confirmed the same value for gold supported on ZnO nanoshapes. The values of the E_{app} (110 ± 5 kJ/mol) over all the Au-containing samples examined here are in close agreement with the previous reports for gold supported on CeO_2 or ZnO. These are shown in the Arrhenius-type plot in Fig. 7. This finding corroborates the conclusion of previous work that the SRM on gold operates by the same mechanism irrespective of the shape (rods vs. cubes of CeO_2; polyhedra vs. rods of ZnO) of a given support or the type (CeO_2, ZnO, ZrO_2) of support; i.e. the support effect is indirect [9–11]. The catalytic reaction takes place on oxidized gold species, Au–O_x. Some supports, such as CeO_2, are superior in binding and dispersing gold atomically; hence their catalytic activity is higher. However, the mechanism is the same; only the number of active sites is varied from support to support. We can therefore anticipate that unsupported nanoporous gold with residual silver impurity [12,13] creating Au–O species will be operating by the same mechanism at an overall activity determined by the number of Au–O-active sites.

SRM reaction rates on gold catalysts at 350 °C are listed in Table 2. On a per gram basis, the rates are significantly different among these four samples. Boucher et al. have reported that the proper scaling of SRM rates on Au/ZnO nanoshapes is by the amount of the polar (0010) surface area of ZnO for samples with the same gold loading [9,10]. As stated above, the number of active Au–O-sites for SRM is crucially related to the number of anchoring points on a support. In ZnO the polar (0010) surfaces are the preferred ones, while in CeO_2 these are the (110) surfaces [9,10]. For the $ZnZrO_x$ system, the amount of highly dispersed ZnO clusters, i.e. the number of anchoring points is correlated to the dispersion of gold, which eventually determines the total reaction rate of the SRM. Spectator gold in the form of particles is loosely bound to the support and inferior in activity for the SRM considering the usage of gold per gram basis. To investigate the fraction of dispersed gold, which has formed the strong Au–O-bonds with the support, leaching with dilute (0.05 wt.%) NaCN aqueous solution for 3 min was performed on all the 1 wt.% Au-containing samples to remove the gold particles. The leachates of the four parent samples (Au/ZnO; Au/$Zn_1Zr_{10}O_x$; Au/leached-$Zn_1Zr_{10}O_x$; and Au/ZrO_2) were tested by ICP to quantify the amount of dissolved Zn and Au during the leaching process, and to back calculate the amount of Au left on each support, which corresponds to the active sites for the SRM reaction on the parent samples. As shown in Table 2, 11.7, 33.0, 48.1 and 53.2% of the original 1 wt.% of gold was retained on Au/ZnO, Au/$Zn_1Zr_{10}O_x$, Au/ZrO_2 and Au/leached-$Zn_1Zr_{10}O_x$, respectively, after cyanide leaching. Rescaling of the

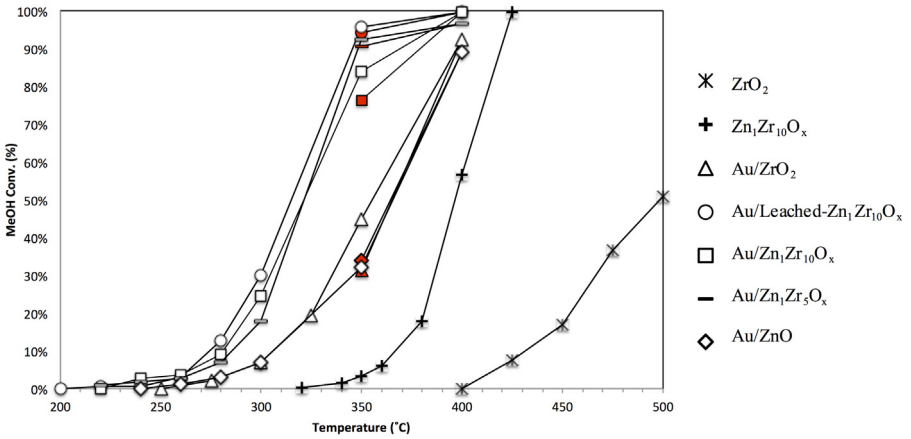

Fig. 6. Methanol conversion in steady-state SRM tests over bare supports and gold-containing samples. Filled symbols are methanol conversions at 350 °C after cooling down from 400 °C. MeOH/H_2O/He molar ratio = 2/2.6/95.4; total flow rate = 50 mL/min, GHSV = 34,000/h.

SRM reaction rate on parent samples at 350 °C by the amount of the residual dispersed gold brings to a closer agreement the turnover frequencies [TOF(Au)], corresponding to CO_2 molecules produced per second per residual gold atoms (Table 2). The E_{app} of the leached Au-containing samples was similar to the E_{app} of the parent catalyst samples (110 ± 5 kJ/mol).

Three cycle of CO-temperature programmed reduction (CO-TPR) were performed on each of the parent and leached samples (Fig. 8), and the results from the last 2 cycles were plotted and averaged for the surface –OH group calculation. Evolution of CO_2 and H_2 corresponds to the active –OH groups which coincides with the activation of Au–O–M species on the metal oxide supports [$-OH + CO \rightarrow CO_2 + 1/2H_2$] [9]. CO-TPR profiles of the four pairs of parent and leached samples indicate the existence of two types of –OH groups activated with peaks at ~250 and ~350 °C, respectively. Low-temperature active –OH groups were found on all the samples with gold atoms, which is attributed to the Au–$(OH)_x$ structures. High-temperature –OH groups, on the other hand, correlate with the less active M–$(OH)_x$ sites. Integration of H_2 peaks shows the amount of –OH groups in units of μmol per gram of catalyst (Table 2) over the whole temperature range up to 400 °C.

The molar ratio of CO_2/H_2 is equal to 2:1 on Au/$Zn_1Zr_{10}O_x$ and Au/leached-$Zn_1Zr_{10}O_x$ samples, while the CO_2/H_2 is found to be 3.1 on Au/ZnO indicating that certain amount of CO_2 is the product of ZnO reduction by CO at high temperature (>350 °C). Dissolving (loss) of some Zn and Au during leaching is the main reason of –(OH) decrease on the leached samples. For Au/leached-$Zn_1Zr_{10}O_x$, the leaching of the bare support before the addition of gold removes most of the excess ZnO that is not well dispersed and bound with ZrO_2. Retaining ZnO in highly dispersed form is less prone to dissolution during the second leaching with dilute NaCN solution, so are the dispersed gold atoms; hence a similar amount of active –OH groups were found for the parent and leached Au/leached-$Zn_1Zr_{10}O_x$. On the other hand, a significant decrease of active –OH groups was observed on Au/$Zn_1Zr_{10}O_x$ after a considerable amount of Au and ZnO was dissolved in the leachate, while the –OH amount on Au/ZnO was low to begin with due to the limited anchoring points on bulk ZnO (Table 2). The SRM turnover frequencies of the parent samples based on the amount of active –OH groups were also calculated and are listed in Table 2. A closer agreement between the four parent samples was observed, indicating that the overall activity of Au-containing samples correlates with the amount of the surface –OH groups surrounding the Au–O–M species. Using the leached samples, we can see from the values of the TOF(Au) and TOF(–OH), footnotes b and d, respectively, in Table 2, that the surface ratio of (OH)/Au atom exceeds 20; even if the actual number is less than that, this finding is important to demonstrate that each Au atom stabilizes a large number of –OH groups around it.

Temperature-programmed oxidation (TPO) of the spent catalyst samples after steady state-SRM was conducted to investigate if any carbon species were present on the surface after reaction [41]. Used samples (none of the used samples shown in Fig. 9 had a black color characteristic of soot deposition) were heated from room temperature to 400 °C for 3 h under 10% O_2/He at the flow rate of 50 mL/min [41]. CO_2 RGA signal intensity was calibrated with the gaseous

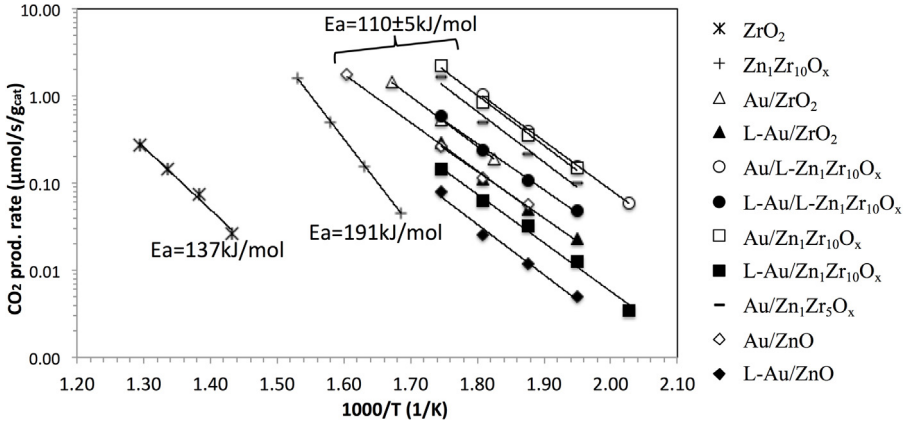

Fig. 7. Arrhenius-type plots for SRM on bare supports and gold-containing (1 wt.%) samples.

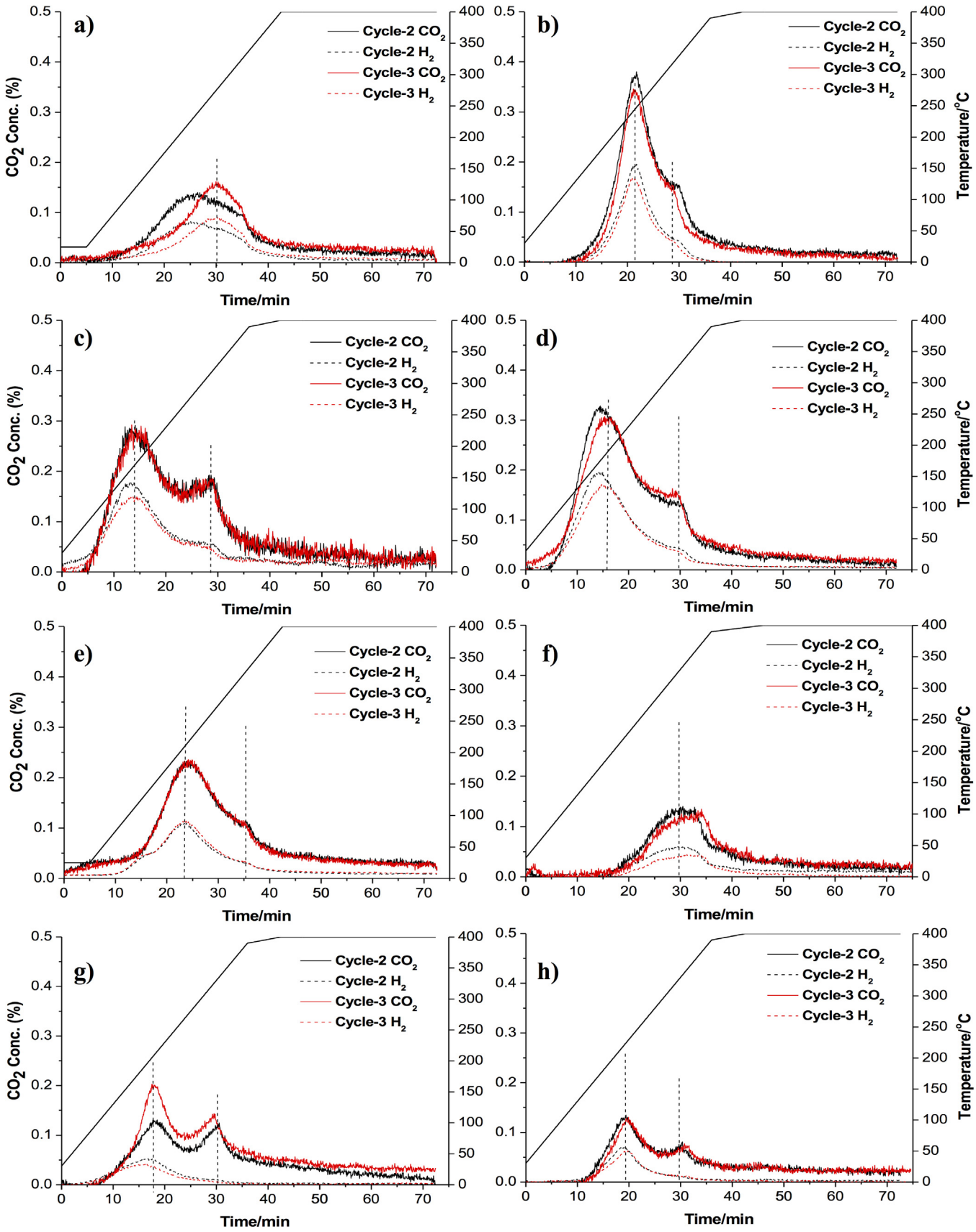

Fig. 8. CO-TPR profiles of a, b) parent and leached Au/ZrO_2; c, d) parent and leached Au/leached-$Zn_1Zr_{10}O_x$; e, f) parent and leached $Au/Zn_1Zr_{10}O_x$; g, h) parent and leached Au/ZnO; CO-TPR conducted in 10% CO/He with the flow rate of 30 mL/min from 30 to 400 °C at the ramping rate of 10 °C/min and holding at 400 °C for 30 min.

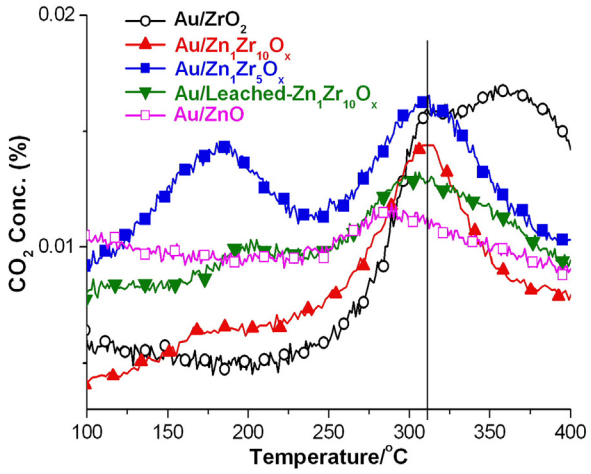

Fig. 9. TPO profiles over used Au-containing samples (after steady-state SRM tests up to 400 °C). Heating from room temperature to 400 °C at 2 °C/min, in 10% O_2/He at the flow rate of 50 mL/min.

concentration of CO_2 in He, and the concentration of CO_2 throughout the TPO test remained below 0.018%, indicating a negligible production of CO_2 from the combustion of carbon species on the surface. A slight increase of CO_2 on Au/leached-$Zn_1Zr_{10}O_x$, Au/$Zn_1Zr_{10}O_x$, and Au/$Zn_1Zr_5O_x$ was observed at 320 °C, while a wider CO_2 peak starting from 300 °C was observed on Au/ZrO_2. No increase of H_2O signal took place at the same temperature range, which indicates that residual carbon species on the catalyst surface is in the form of carbonates, not hydrocarbons.

3.4. Temperature-programmed surface reaction tests

Temperature-programmed surface reaction tests coupled with mass spectrometry (TPSR/MS) were conducted to study the reaction under dynamic conditions (Fig. 10). In the case of methanol dehydrogenation (when no H_2O is used), the TPSR method can be useful in capturing stable intermediates, such as methyl formate [9],which elucidate the mechanism of the reaction. CH_3OH-TPSR data (not shown here) on both Au/ZrO_2 and Au/$Zn_1Zr_{10}O_x$ samples have identified the formation of methyl formate via methanol coupling ($2CH_3OH \rightarrow HCOOCH_3 + 2H_2$) by MS. Methyl formate as an intermediate is short-lived and readily oxidized by water to form formic acid, therefore in SRM-TPSR it is not captured by MS. Only in the absence of water will methyl formate be detected, which was found to be true also in other Au/MO systems studied previously by our group [10,11,15]. It has also been reported to form in the selective oxidation of methanol on the nanoporous gold catalysts recently studied by Friend and co-workers [12,13]. The latter work states that direct oxidation of CH_3O– by –OH is not likely to occur due to the rapid deprotonation of methoxy groups to formaldehyde and the nucleophilic property of both the methoxy and hydroxide groups [42].

To investigate the role of H_2O on methanol reforming, ($CH_3OH + H_2O$)-TPSR was conducted on all Au-containing samples. Simultaneous production of H_2 and CO_2 started at 250 °C on Au/ZrO_2 sample, while at ~300 °C, CO started to be produced. This narrow temperature window for exclusive $H_2 + CO_2$ production (selectivity > 99%) is due to the weak binding between gold and bare ZrO_2. As temperature increases to 300 °C and above, the catalysis by ZrO_2 surface strong Lewis acid sites takes over [30,43], i.e. methanol decomposition occurs through the CO and H_2 pathway. Great enhancement by ZnO-modification was observed on Au/$Zn_1Zr_{10}O_x$ and Au/leached-$Zn_1Zr_{10}O_x$ samples, where simultaneous H_2 and CO_2 production started at below 225 and 200 °C, respectively. Exclusive production of $H_2 + CO_2$ was maintained up to 375 and 325 °C, respectively, where CO started to be produced. This wider temperature window for CO-free SRM reaction is due to the modification of the ZrO_2 surface to "ZnO-like", as the IPA-TPD tests have demonstrated. ZnO catalyzes the CO-free SRM at

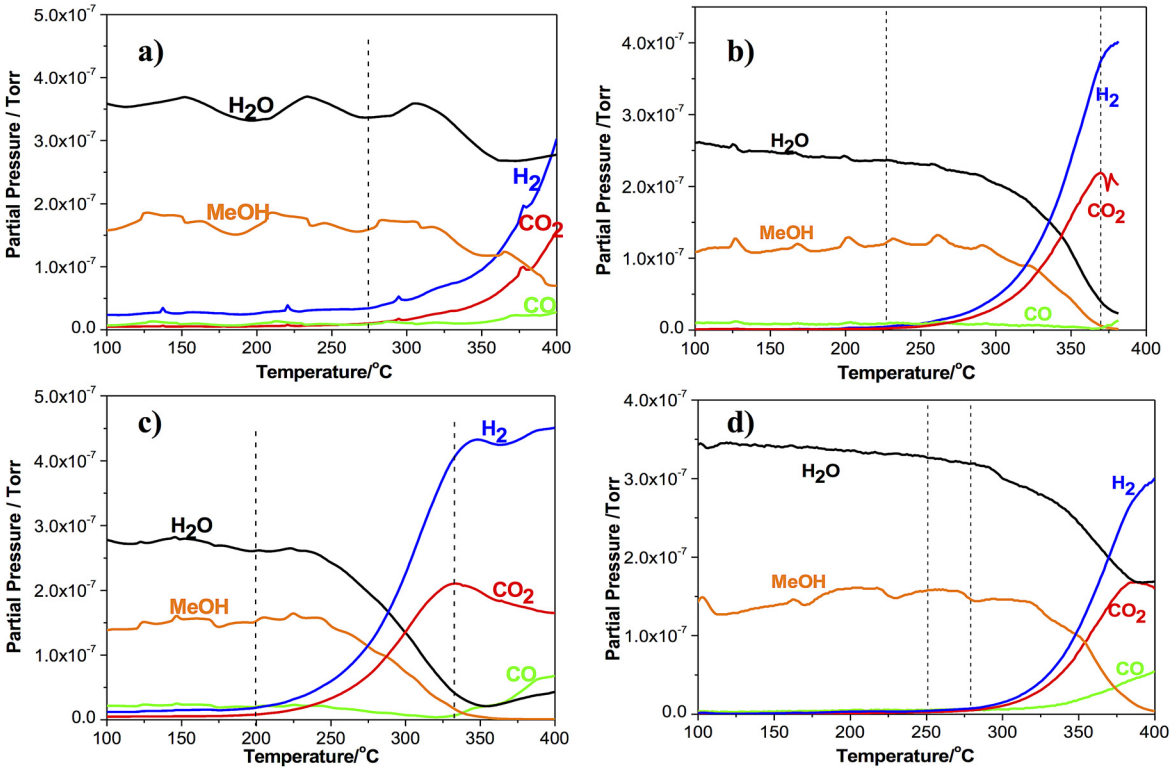

Fig. 10. SRM-TPSR on a) 1 wt.% Au/ZnO; b) 1 wt.% Au/$Zn_1Zr_{10}O_x$; c) 1 wt.% Au/leached-$Zn_1Zr_{10}O_x$; d) 1 wt.% Au/ZrO_2

temperatures above 300 °C [9,10]. However, the composite $ZnZrO_x$ surface has superior activity to bulk ZnO as the light-off temperature of SRM on Au/ZnO is 275 °C, which is higher than for Au on the $ZnZrO_x$ supports (Fig. 10). This is due to the larger number of active Au–O-species on the latter than on the former, as discussed above.

Overall, therefore, we have found that modification of ZrO_2 by addition of ~10 at.% ZnO by the carbon hard-template method creates a superior support for gold, whereby highly dispersed ZnO clusters are strongly coupled with the ZrO_2 nanocrystals, and provide many more anchoring sites for the gold catalyst species than bulk ZnO. Furthermore, the modification benefits the selectivity to H_2 over a wider temperature window (to ~375 °C), as the ZrO_2 acid sites are passivated by ZnO and the surface is "ZnO-like". As an added feature, ZnO stability is improved and gold remains anchored stably after reaction. In summary, ZnO-modified ZrO_2 is an attractive support for gold catalysts, maintaining high activity and high CO_2 and H_2 selectivity during low- and moderately-high SRM reaction temperatures.

4. Conclusions

To our knowledge, this work is a first demonstration of how to use a ZnO-modified ZrO_2 as a support for gold catalysts for the low-temperature SRM reaction. Modification of ZrO_2 by ZnO-addition passivates the strong acidity of ZrO_2, and simultaneously creates anchoring sites on the highly dispersed ZnO clusters for Au–O-species to strongly bind and activate methanol. The typical high activity of Au–O-species for the SRM reaction, as well as their exclusive selectivity to H_2 and CO_2 (up to 350 °C) are manifested on the $ZnZrO_x$ support. The surface modification of ZrO_2 by ZnO also renders the ZnO clusters on the ZrO_2 much more conducive to binding gold atoms; hence they are more efficiently utilized than bulk ZnO nanoparticles. Overall, this method offers a way to improve activity by creating many more active Au–O-sites on the dispersed ZnO clusters, but also it improves stability, as the composite $ZnZrO_x$ phase resists sintering and is non-leachable in highly alkaline solutions. A generalized use of this type of surfaces for other metals, such as copper, is recommended for applications to methanol reactions, the water–gas shift and other such systems where the metal catalyst should be stabilized in atomically dispersed state on supports.

Conflict of interest statement

The authors declare no conflict of interest.

Acknowledgments

The financial support of this work by the U.S. Department of Energy, Basic Energy Sciences, under Grant DE-FG02-05ER15730 is gratefully acknowledged. C.W. thanks Dr. Y. Zhang and Dr. S. Speakman at MIT's Center for Material Science and Engineering for their assistance with TEM and XRD; and Dr. H. Lin at Harvard University's Center for Nanoscale Systems for his assistance with XPS. M.Y. thanks Dr. L. Allard of Oak Ridge National Laboratory for his assistance with the ac-HAADF/STEM work.

References

[1] J. Larminie, A. Dicks, Fuel Cell Systems Explained, second ed., Wiley, Chichester, UK, 2003.
[2] R.M. Navarro, M.A. Pena, J.L.G. Fierro, Chem. Rev. 107 (2007) 3952–3991.
[3] L. Bromberg, W.K. Cheng (Eds.), Methanol as an Alternative Transportation Fuel in the US: Options for Sustainable and/or Energy-Secure Transportation Final Report, Massachusetts Institute of Technology, Cambridge, MA, 2010, p. 78.
[4] S. Sa, H. Silva, L. Brandao, J.M. Sousa, A. Mendes, Appl. Catal. B Environ. 99 (2010) 43–57.
[5] F. Menegazzo, F. Pinna, M. Signoretto, V. Trevisan, F. Boccuzzi, A. Chiorino, M. Manzoli, ChemSusChem 1 (2008) 320–326.
[6] Y. Matsumura, H. Ishibe, Appl. Catal. B Environ. 91 (2009) 524–532.
[7] J.P. Breen, J.R.H. Ross, Catal. Today 51 (1999) 521–533.
[8] B. Lindstrom, L.J. Pettersson, P. Govind Menon, Appl. Catal. A Gen. 234 (2002) 111–125.
[9] M.B. Boucher, S. Goergen, N. Yi, M. Flytzani-Stephanopoulos, PCCP 13 (2011) 2517–2527.
[10] N. Yi, M.B. Boucher, F. Gittleson, B. Zugic, H. Saltsburg, M. Flytzani-Stephanopoulos, J. Phys. Chem. C 115 (2011) 1261–1268.
[11] N. Yi, R. Si, H. Saltsburg, M. Flytzani-Stephanopoulos, Energy Environ. Sci. 3 (2010) 831–837.
[12] B. Xu, J. Haubrich, C.G. Freyschlag, R.J. Madix, C.M. Friend, Chem. Sci. 1 (2010) 310–314.
[13] A. Wittstock, V. Zielasek, J. Biener, C.M. Friend, M. Bäumer, Science 327 (2010) 319–322.
[14] K.M. Kosuda, A. Wittstock, C.M. Friend, M. Bäumer, Angew. Chem. Int. Ed. 51 (2012) 1698–1701.
[15] N. Yi, R. Si, H. Saltsburg, M. Flytzani-Stephanopoulos, Appl. Catal. B Environ. 95 (2010) 87–92.
[16] N. Yi, H. Saltsburg, M. Flytzani-Stephanopoulos, ChemSusChem 6 (2013) 816–819.
[17] Q. Fu, H. Saltsburg, M. Flytzani-Stephanopoulos, Science 301 (2003) 935–938.
[18] Q. Fu, W. Deng, H. Saltsburg, M. Flytzani-Stephanopoulos, Appl. Catal. B Environ. 56 (2005) 57–68.
[19] W. Deng, C. Carpenter, N. Yi, M. Flytzani-Stephanopoulos, Top. Catal. 44 (2007) 199–208.
[20] M. Manzoli, A. Chiorino, F. Boccuzzi, in: A. Gamble, C. Colella, S. Coluccia (Eds.), Oxide Based Materials: New Sources, Novel Phases, New Applications, Elsevier Science B.V., Amsterdam, The Netherlands, 2005, pp. 405–413.
[21] N. Takezawa, N. Iwasa, Catal. Today 36 (1997) 45–56.
[22] X. Zhang, H. Wang, B.-Q. Xu, J. Phys. Chem. B 109 (2005) 9678–9683.
[23] C.-M. Wang, K.-N. Fan, Z.-P. Liu, J. Am. Chem. Soc. 129 (2007) 2642–2647.
[24] M. Manzoli, F. Boccuzzi, V. Trevisan, F. Menegazzo, M. Signoretto, F. Pinna, Appl. Catal. B Environ. 96 (2010) 28–33.
[25] F. Zane, V. Trevisan, F. Pinna, M. Signoretto, F. Menegazzo, Appl. Catal. B Environ. 89 (2009) 303–308.
[26] J. Li, N. Ta, W. Song, E. Zhan, W. Shen, gold bulletin 42 (2009) 48–60.
[27] K.-H. Jacob, E. Knozinger, S. Benier, J. Mater. Chem. 3 (1993) 651–657.
[28] K. Tanabe, M. Misono, Y. Ono, H. Hattori, New Solid Acids and Bases: Their Catalytic Properties, Elsevier, Amsterdam, The Netherlands, 1989.
[29] J. Sun, K. Zhu, F. Gao, C. Wang, J. Liu, C.H.F. Peden, Y. Wang, J. Am. Chem. Soc. 133 (2011) 11096–11099.
[30] M. Badlani, I.E. Wachs, Catal. Lett. 75 (2001) 137–149.
[31] J.D. Lessard, I. Valsamakis, M. Flytzani-Stephanopoulos, Chem. Commun. 48 (2012) 4857–4859.
[32] R. Srinivasan, R.J. De Angelis, G. Ice, B.H. Davis, J. Mater. Res. 6 (1991) 1287–1292.
[33] C.H. Lu, J.M. Raitano, S. Khalid, L.H. Zhang, S.W. Chan, J. Appl. Phys. 103 (2008) 7.
[34] C.-C. Chen, W.-Y. Cheng, S.-Y. Lu, Y.-F. Lin, Y.-J. Hsu, K.-S. Chang, C.-H. Kang, K.-L. Tung, CrystEngComm 12 (2010) 3664–3669.
[35] A. Hugon, N.E. Kolli, C. Louis, J. Catal. 274 (2010) 239–250.
[36] R. Zanella, S. Giorgio, C.R. Henry, C. Louis, J. Phys. Chem. B 106 (2002) 7634–7642.
[37] M.C.I. Bezen, C. Breitkopf, N. El Kolli, J.-M. Krafft, C. Louis, J.A. Lercher, Chem. Eur. J. 17 (2011) 7095–7104.
[38] A. Gervasini, J. Fenyvesi, A. Auroux, Catal. Lett. 43 (1997) 219–228.
[39] A. Gervasini, A. Auroux, J. Catal. 131 (1991) 190–198.
[40] T. Tago, H. Konno, M. Sakamoto, Y. Nakasaka, T. Masuda, Appl. Catal. A Gen. 403 (2011) 183–191.
[41] W. Deng, M. Flytzani-Stephanopoulos, Angew. Chem. Int. Ed. 45 (2006) 2285–2289.
[42] B. Xu, X. Liu, J. Haubrich, C.M. Friend, Nat. Chem. 2 (2010) 61–65.
[43] J.M. Tatibouet, Appl. Catal. A Gen. 148 (1997) 213–252.